A Study into Effects of CO_2 Laser Melting of Nitrided Ti-6Al-4V Alloy

M.A. Mohammed, M.S.J. Hashmi, and B.S. Yilbas

Multiple treatment of engineering surfaces can provide improved surface properties that cannot be obtained by a single surface treatment. Consequently, this study investigates the effects of laser melting on the microstructures of plasma nitrided Ti-6Al-4V alloy. The study consists of two parts. In the first part, governing equations pertinent to the laser melting process are developed, and temperature variation across the melted zone is predicted. In the second, an experiment is conducted to nitride the surface of the alloy through plasma nitriding process and to melt the plasma nitrided and the untreated alloy surfaces with a CO_2 laser beam. The resulting metallurgical changes are examined using x-ray diffraction (XRD), energy-dispersive spectrometry (EDS), and scanning electron microscopy (SEM) techniques. It is shown that three distinct nitride layers are formed in the vicinity of the alloy surface prior to the laser melting process, and that after the melting process nitrided species are depleted while cellular and dendritic structures are formed. In addition, the structure consisting of transformed β containing coarse and fine acicular α is observed in the melted regions.

Keywords plasma nitriding, laser melting, titanium alloy

Introduction

Alloy Ti-6Al-4V is used widely in industry because of its low density and high toughness/mass ratio. Due to low wear properties at the surface, several techniques have been considered to improve tribological properties of the alloy. These include: plasma nitriding, coating, and carbonizing (Ref 1-3). The basic concept in using plasma nitriding to improve the surface properties of a titanium material is the possibility of forming nitride species at and below the surface. Titanium nitrides are hard materials that can increase the wear resistance of the alloy. It is documented that when nitrogen forms a solid solution as a consequence of plasma nitriding in titanium alloys, it results in hardening through a dislocation pinning mechanism (Ref 4). The main advantages of the plasma nitriding include: thick layer of nitride formation in the vicinity of the surface and high reproducibility.

On the other hand, because of the brittleness of the resulting compound layer formed at substance surface, a secondary surface treatment becomes fruitful for plasma nitrided materials. Increasing demand is evident in laser processing to improve the wear resistance of the substance (Ref 5). In surface processing with a laser beam, a surface area of the substance is scanned through a moving laser source. Because of the high power absorbed by the substance surface, melting of the surface takes place. Moreover, solidification occurs during the cooling cycle, which in turn results in metallurgical changes in the resolidified region that differs from the original surface. This process may provide improved mechanical and wear properties (Ref 6). Moreover, duplex surface treatment of 1 to 5% Cr steel was carried out by Zenker (Ref 7). Initially, steel was nitrocarburized before laser treatment. It was shown that considerable increase in effective case depth was obtained. Q-switched laser alloying carbon into copper alloys for enhanced corrosion properties was carried out by Sawchyn and Draper (Ref 8). They showed that the corrosion properties increased considerably after the laser alloying process. Consequently, investigation into secondary treatment of engineering surfaces becomes fruitful, since multiple treatment of a surface can introduce properties of a surface that are unobtainable through any single surface treatment process.

In this study, the heating model appropriate to laser heating process was introduced theoretically while laser melting of Ti-6Al-4V workpieces subject to plasma nitriding was carried out experimentally. A plasma nitriding unit was used to nitride the workpiece surfaces up to a depth of 40 μm and CO_2 laser delivering 1.2 kW nominal output was used to irradiate the workpiece surfaces. X-ray diffraction (XRD), scanning electron microscopy (SEM), and energy-dispersive x-ray spectrometry (EDS) were carried out to examine the laser-induced metallur-

M.A. Mohammed, RED, URMD, Saudi Aramco, Dhahran, Saudi Arabia; **M.S.J. Hashmi,** School of M&M Engg. Dublin City University, Dublin, Ireland; and **B.S. Yilbas,** ME Department KFUPM, Dhahran, Saudi Arabia.

Nomenclature

C_p	Specific heat capacity, J/kg · K
I	Power intensity of laser beam, W/m^2
k	Thermal conductivity, @/m · K
k_B	Boltzmann's constant
L	Enthalpy of evaporation, kJ/kg
m	Atomic weight, kg
t	Time, s
T	Temperature, K
T_s	Surface temperature, K
V	Instantaneous velocity of evaporating front, m/s
x	Distance from the surface, m
α	Thermal diffusivity, m^2/s
δ	Absorption depth, 1/m
ρ	Density, kg/m^3

gical changes for both laser-treated and untreated workpieces. Moreover, the predictions obtained from the heating model were then related to experimental findings.

Heat Transfer Model

Laser heating can be modeled analytically when introducing the following assumptions:

- Thermionic emission is neglected.
- Surface temperature should be kept below (~4000 K); therefore, no plasma is formed by irradiation from target surface.
- Absorption process is governed by Lambert's law.
- Thermal properties are kept constant.

The Fourier equation governing the laser heating process can be written as (Ref 9):

$$k\left(\frac{\partial^2 T}{\partial x^2}\right)+\rho C_p V\frac{\partial T}{\partial x}+I_0\delta\exp(-\delta x)=\left(\frac{\partial T}{\partial t}\right)\rho C_p T \qquad \text{(Eq 1)}$$

where:

$$V=\left(\frac{k_B T_s}{2\pi m}\right)^{1/2}\exp\left(-\frac{L}{k_B T_s}\right) \qquad \text{(Eq 2)}$$

It is evident that the problem is nonlinear, since the evaporating front velocity V is changing with time. Consequently, complete solution of the heat transfer equation is extremely difficult, but quasi-steady solution is feasible. The set of boundary conditions relevant to Eq 1 and 2 is:

$$k\frac{dT}{dx}\Big|_{x=0}=\rho VL;\ \text{and}\ T(\infty,t)=0\ \text{and}\ T(x,0)=0 \qquad \text{(Eq 3)}$$

The solution of Eq 1 and 2 with the appropriate boundary conditions can be obtained using a Laplace transformation. The mathematical arrangements of the Laplace transformation are given in the Appendix to this article. The solution of the heat transfer equation yields:

Table 1 Plasma nitriding conditions

Temperature, °C	450-520
Time, ks	54-72
Voltage (dc), V	400-700
Total pressure, kPa	0.46-0.51

Table 2 Laser and assisting gas parameters

Laser output power, kW	Helium-assisting gas pressure, kPa
1.2	125
1.6	185

$$T(x,t)=\frac{I_0\delta\sqrt{\alpha}}{2\rho C_p(\alpha\delta-V)}\left\{4\sqrt{t}\ \text{ier fc}\left(\frac{x}{2\sqrt{\alpha t}}+b\sqrt{t}\right)+\frac{3b^2+c^2}{2b(\quad\ \ -\quad)}\right.$$
$$\text{erfc}\left(\frac{x}{2\sqrt{\alpha t}}+b\sqrt{t}\right)+\frac{1}{2b}\exp\left(-\frac{2bx}{\sqrt{\alpha}}\right)\text{erfc}\left(\frac{x}{2\sqrt{\alpha t}}-b\sqrt{t}\right)$$
$$+\frac{1}{(b-c)}\exp\left[-(\delta x+(b^2-c^2)t)\right]\text{erfc}\left[-\left(\frac{x}{2\sqrt{\alpha t}}+c\sqrt{t}\right)\right]$$
$$-\frac{1}{(b-c)}\exp\left[-\frac{x}{\sqrt{\alpha}}(b+c)+(b^2+c^2)t\right]$$
$$\left.\text{erfc}\left(\frac{x}{2\sqrt{\alpha t}}-c\sqrt{t}\right)-\frac{2}{(b-c)}\exp(-\delta x)\right\}$$
$$-\frac{\rho VL}{4bk}\left\{4b\sqrt{\alpha t}\ \text{ierfc}\left(\frac{x}{2\sqrt{\alpha t}}+b\sqrt{t}\right)-\sqrt{\alpha}\right.$$
$$\text{erfc}\left(\frac{x}{2\sqrt{\alpha t}}+b\sqrt{t}\right)+\sqrt{\alpha}\exp\left(-\frac{2bx}{\sqrt{\alpha}}\right)$$
$$\left.\text{erfc}\left(\frac{x}{2\sqrt{\alpha t}}-b\sqrt{t}\right)\right\} \qquad \text{(Eq 4)}$$

Setting $x = 0$ in Eq 4 results in the surface temperature, that is:

$$T(0,t)=\frac{I_0\delta\sqrt{\alpha}}{2\delta C_p(\alpha\delta-V)}\left(4\sqrt{t}\ \text{ier fc}(b\sqrt{t})+\frac{(b^2+c^2)}{b(b^2-c^2)}\text{erfc}\,(b\sqrt{t})\right.$$
$$+\frac{1}{b}+\frac{\exp[(b^2-c^2)t]}{(b-c)}\text{erfc}\,(-c\sqrt{t})-\frac{\exp[-(b^2-c^2)t]}{(b+c)}$$
$$\left.\text{er fc}\,(-c\sqrt{t})-\frac{2}{(b-c)}\right)-\frac{\rho VL}{4bk}[4b\sqrt{\alpha t}\ \text{ier fc}\,(b\sqrt{t})$$
$$-\sqrt{\alpha}\ \text{erfc}\,(b\sqrt{t})+\sqrt{\alpha}\,(2-\text{erfc}\,(b\sqrt{t}))]$$

Rearrangement gives:

$$T(0,t)=\frac{I_0\delta\sqrt{\alpha}}{2\rho C_p(\alpha\delta-V)}\left(4\sqrt{t}\ \text{ierfc}\,(b\sqrt{t})+\frac{(b^2+c^2)}{b(b^2-c^2)}\text{er fc}\,(b\sqrt{t})\right.$$
$$\left.+\frac{2c}{b^2-c^2}\exp\,[-(b^2-c^2)t]\,\text{erfc}\,(-c\sqrt{t})-\frac{(b+c)}{b(b-c)}\right)$$
$$-\frac{\rho VL}{2bk}[2b\sqrt{\alpha t}\ \text{ier fc}\,(b\sqrt{t})+\sqrt{\alpha}\ \text{erfc}\,(b\sqrt{t})] \qquad \text{(Eq 5)}$$

Equations 4 and 5 are the complete quasi-steady solution of the governing equation and can be used to form the basis for a more accurate solution, which can be obtained by an iterative procedure. It is expected that this solution would be obtained by developing the solution from time $t = 0$. In the initial stages, the evaporation rates are small and thus the solution is for the pure conduction process. As the surface temperature rises, so does the evaporation rate. The values for the velocity and surface temperature can be obtained by stepping forward in time using time steps that are small enough that the change in the surface velocity between steps is small and therefore the velocity de-

rived in the previous step can be used directly in Eq 5. With this new value of the surface temperature, an improved estimate of the surface velocity (V) can be obtained, and the iteration repeated to give a convergent solution. A computer program was developed to obtain the temperature profiles at the surface and inside the substance.

Experimental

Plasma nitriding was achieved with a –700 Vdc bias voltage. The nitriding conditions are given in Table 1. Prior to the nitriding process, workpieces were polished and ultrasonically cleaned; moreover, the sputtering technique was used to clean the surfaces in argon and hydrogen (3/1) plasma for 45 min.

A CO_2 laser with nominal output power of 1.2 kW was used to irradiate the nitrided and untreated workpiece surfaces. During melting process, helium was used as a shielding gas. In order to achieve low and high melting regions, the laser output power intensity was varied. It should be noted that high melting corresponds to the melting occurring at a temperature between the melting and the evaporation temperatures, while low melting corresponds to the melting occurring at the melting temperature. The laser output power and shielding gas pressure in relation to the melting process are given in Table 2.

X-ray diffraction was carried out to analyze the nitride species in the melted and untreated regions, while EDS was conducted to obtain the elemental distribution in those regions. Scanning electron microphotography was carried out to examine the metallurgical changes in the melted regions.

Results and Discussion

The variation of surface temperature with time is shown in Fig. 1. After the start of melting, surface temperature rapidly increases to reach the evaporation temperature. This may be due to heat transfer taking place inside the material, that is, electrons close to the surface absorbing the incident laser radiation and transferring their excess energy to the substance through increased rate of conduction. In this case, internal energy of the substrate increases due to increased rate of absorbed energy, which in turn gives rise to high surface temperature. Once the evaporation temperature is reached, almost equal energy distribution among the heat conduction, convection, and melting processes occurs in the vicinity of the surface; that is, energy balance occurs among the energy gain from the laser beam and heat losses caused by convection and evaporation processes, which in turn results in constant temperature.

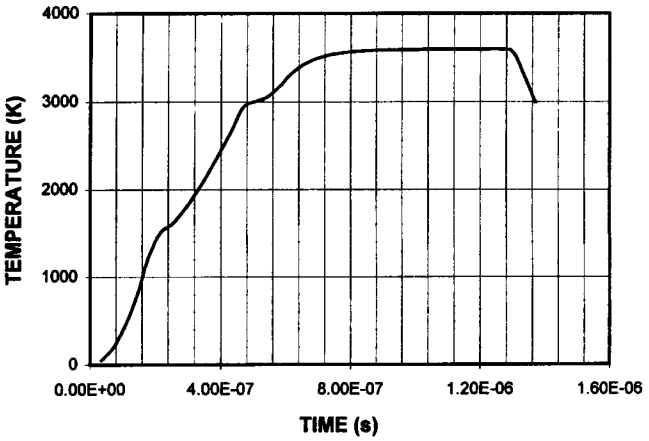

Fig. 1 Surface temperature rise (predicted from theory) with time

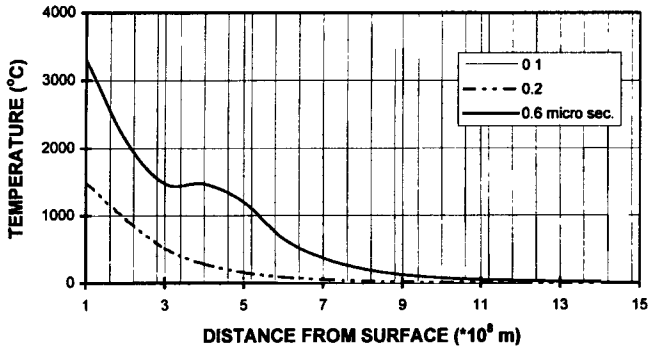

Fig. 2 Temperature profiles inside the substance predicted from theory

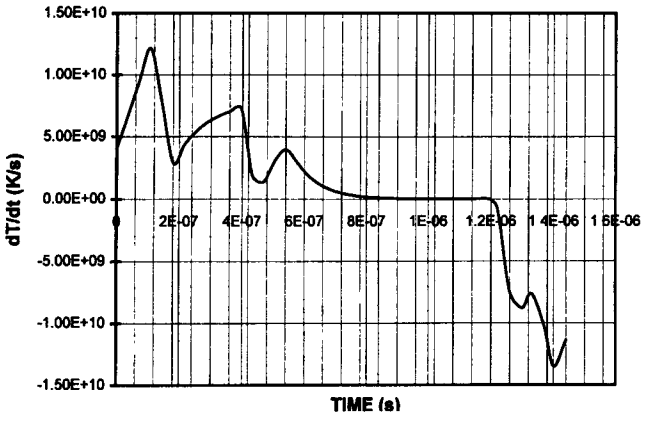

Fig. 3 Variation of dT/dt with time predicted from theory

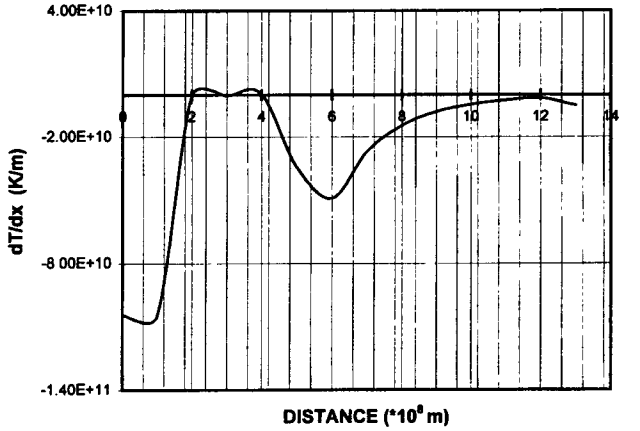

Fig. 4 Variation of dT/dx with distance predicted from theory

Figure 2 shows the temperature profile inside the substance. Initially, the temperature profile is considerably flat, but as the heating progresses, the profile changes with maximum temperature occurring at the surface. At the onset of melting, the point of the maximum temperature extends inside the material. This is because the convection effect is dominant at the surface, resulting in an almost constant temperature gradient developed at the surface. However, once the evaporation initiates at the surface, then the negative temperature gradient develops at the surface. This indicates that the temperature below the surface reaches the maximum and further increase in heating causes liquid metal to reach a higher temperature in this region than that corresponding to the surface. In this case, superheating dominates the heat conduction, resulting in a nonequilibrium transient process underneath the surface. Consequently, the melting occurring in this region is called a high melting region, while melting occurring at the melting temperature is called the low melting region. The low and high melting regions are also evident from SEM micrographs (Fig. 7).

The variation of temperature gradient (dT/dt) with time is shown in Fig. 3. The slope of the curve changes considerably with heating time. As the heating progresses toward the end of the laser pulse, the energy losses due to conduction and convection are dominant and energy gains from a laser source are less significant compared to the energy losses. In this region, cooling cycle is initiated and a cooling rate of almost 10^6 K/s is evident. The variation of temperature gradient (dT/dx) with distance is shown in Fig. 4. Two regions are visible. In the first region (closer to the surface), rapid variation in dT/dx occurs; in this case, high melting region results. However, in the second region , dT/dx shows smaller variation as compared to the first region; in this case, low melting region results.

Scanning electron microscopy results for plasma nitrided samples are shown in Fig. 5. Three distinct zones are evident from the photographs. These include compound layer, inner layer, and outer layer. The thickness of these layers extends to about 8 μm for compound layer, 12 μm for inner layer, and 20 μm for outer layer. The XRD results for plasma nitrided samples are shown in Fig. 6. The nitrided samples exhibit diffraction lines of δTiN and εTi_2N phases. The weight fraction of these phases varies within the nitrided layer and indicate that the concentration of the δ phase decreases with the depth, while αTi concentration increases. In the compound layer εTi_2N + δTiN phases occur. In the inner layer α(TiN) with or without ε phase occurs. In the outer layer, nitride precipitates are dominant.

X-ray diffraction results for the plasma/laser melted workpieces are shown in Fig. 6, while SEM results for the nitrided/laser melted workpieces are shown in Fig. 7. It is evident that nitride compounds almost disappear because of the heating effect in the case of high melting region. Because the melting is carried out under shielding gas, the effect of oxygen is minimal and no oxygen compound is evident from XRD results. It is evident from SEM micrographs (Fig. 7) that the rapid solidifica-

Table 3 Elemental distribution in laser melted regions

	Distribution, wt%						
	Al	V	Cu	Cr	Fe	O	Ti
No treatment	6	4	0.03	0.01	0.32	0.2	bal
Laser melted low-melt region	5	4	0.03	0.01	0.32	Unknown	bal
Laser melted high-melt region	3	4.5	0.03	0.01	0.3	Unknown	bal

bal, balance

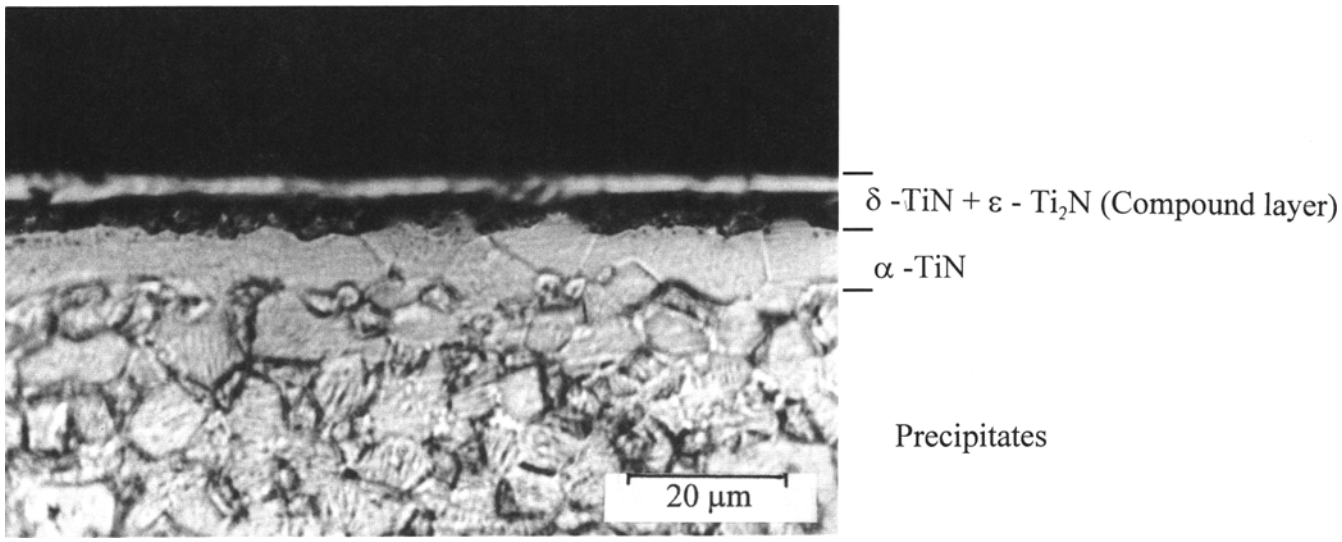

Fig. 5 Microphotograph of plasma nitrided workpiece cross section

tion caused by a high cooling rate produces acicular α, which is finer than the platelike α, and a prior β grain boundary is also seen. Moreover, for relatively low cooling rate, the structure consists of transformed β containing acicular α: α at prior β grain boundaries can be observed. In addition, the structure consists of transformed β containing coarse and fine acicular α is evident. The heat-affected zone in the treated workpieces possesses primarily α′ martensite. However, α + β microstructure is found in the unaffected region. In general, laser-treated surfaces consist of cellular and dendritic structures, that is, at high cooling rates cellular structures are evident and are obscured by α′ martensite (Ref 11). It is evident from XRD tests that the dendritic region of the nitrided workpiece consists of TiN.

Figure 8 shows EDS spectrum, while Table 3 gives the elemental distribution in laser melted and untreated regions. It can be seen that aluminum depletes in the high melting region. Moreover, titanium depletion in both high and low melting regions is small. The depletion in aluminum can be attributed to its low melting and evaporation temperatures. In this case, it is expected that aluminum may be ejected because of the melt pressure developed in the high melting region.

Conclusions

Plasma nitriding results in three distinct nitride zones in the vicinity of the surface. These include compound layer (εTi_2N + δTiN phase occurs), inner layer (αTiN with or without ε-phase develops), and outer layer where precipitates are dominant. However, after laser heating process, nitride species almost disappears, which is especially true for high-melting regions.

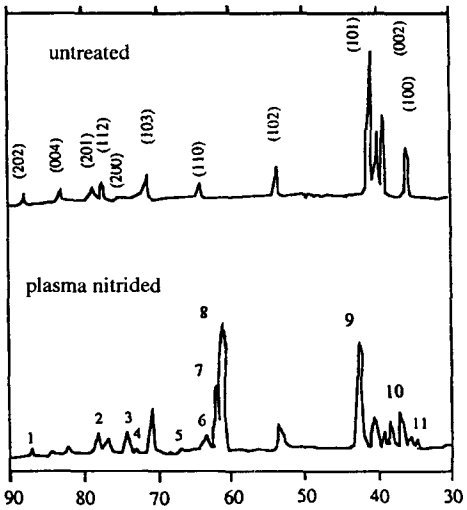

1	2	3	4	5	6	7	8	9	10	11
ε-Ti2N (302)	δ-TiN (222)	δ-TiN (311)	ε-Ti2N (202)	ε-Ti2N (311)	ε-Ti2N (102)	δ-TiN (220)	ε-Ti2N (002)	δ-TiN (200)	δ-TiN (111)	ε-Ti2N (101)

Fig. 6 XRD results for plasma nitrided workpiece

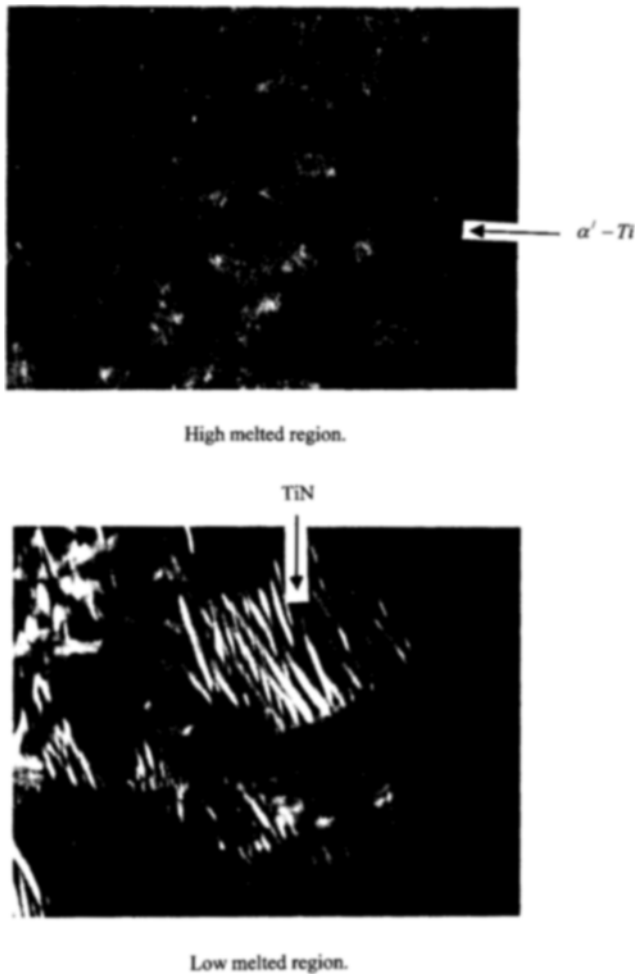

Fig. 7 Microphotographs of laser melted regions

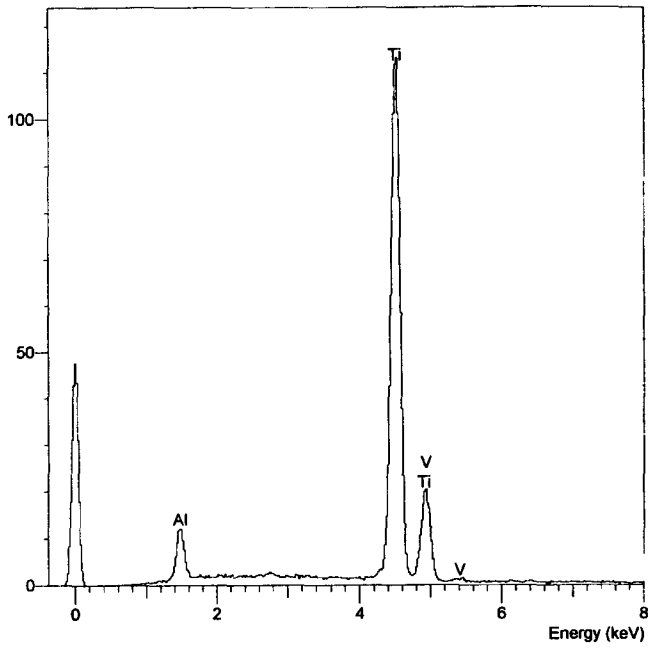

Fig. 8 EDS spectrum

The oxide compound is not seen, because the laser melting process was carried out at shielding ambient.

The rapid solidification caused by a high cooling rate produces acicular α. However, in the case of low-melting regions, the structure consists of transformed β containing acicular α: α at prior β grain boundaries can be observed. The heat-affected zone possesses primarily α′ martensite. As it is expected, α + β structure is evident in the unaffected region. Cellular and dendritic structures occur in the laser melted regions.

Depletion in aluminum occurs in the laser melted regions. Moreover, depletion in titanium in the high-melting region is evident. However, this occurs rarely in a small rate. Aluminum depletion may be explained in terms of its low melting and evaporation temperatures.

References

1. A. Gicquel, N. Laidani, P. Saillard, and I. Amauroux, Plasma and Nitrides: Application to the Nitriding of Titanium, *Pure Appl. Chem.*, Vol 62 (No. 9), 1990, p 1743-1750
2. M. Zlatanovic, T. Gredic, N. Popovic, and Z. Bogdanov, Matching of TiN Coating Structures by Plasma Nitriding of Substrates, *Vacuum*, Vol 44 (No. 2), 1993, p 83-88
3. A. Muche and M. Braun, Requisite Parameters for Optimal Wear Performance of Nitrogen Implanted Titanium and Ti-6Al-4V, *Surf. Coat. Technol.*, Vol 50, 1992, p 135-139
4. N. Laidani, J. Perriere, D. Lincot, A. Gicquel, and J. Amauroux, Nitriding of Bulk Titanium and Thin Titanium Films in a NH_3 Low Pressure Plasma, *Appl. Surf. Sci.*, Vol 36, 1989, p 520-529
5. B.L. Mordike, State of the Art of Surface Engineering with High Energy Beams, *Key. Eng. Mater.*, Vol 46, 47, 1990, p 13-26
6. T. Bell, M.H. Sohi, J.R. Betz, and A. Bloyce, Energy Beams in Second Generation Surface Engineering of Aluminum and Titanium Alloys *Key Eng. Mater.*, Vol 46, 47, 1990, p 69-84
7. R. Zenker and U. Zenker, Combined Heat Treatment of Steel: Nitrocementation and Laser Treatment, *Phys. Met. Metallogr.*, Vol 66 (No. 6), 1968, p 97-105
8. I. Sawchyn and C.W. Draper, AES and RBS Analysis of Laser Mixed Cr and Ni Multilayer Films on Cu Alloys, *Appl. Surf. Sci.*, Vol 18 (No. 1-2), 1984, p 86-105
9. B.S. Yilbas, A.Z. Sahin, and R. Davier, Laser Heating Mechanism Including Evaporation Process Initiating Laser Drilling, *Int. J. Mech. Tools Manufact.*, Vol 35 (No. 7), 1995, p 1047-1062
10. B.S. Yilbas and A.Z. Al-Garni, Some Aspects of Laser Heating of Engineering Materials, *J. Laser Appl.*, Vol 8, 1996, p 197-204
11. J. Folhers, D.R.F. West, and W.M. Steen, Laser Surface Melting and Alloying of Titanium, *Laser Surface Treatment of Metals*, Vol 6, 1986, p 451-460

Appendix

The solution of Eq 1 and 2 with the appropriate boundary conditions can be obtained using a Laplace transformation with respect to time t, as follows.

The governing equation is:

$$\frac{\partial^2 T(x,p)}{\partial x^2} + \frac{V}{\alpha}\frac{\partial T(x,p)}{\partial x} - \frac{p}{\alpha}T(x,p) = -\frac{I_0\delta}{kp}\exp(-\delta x) \quad \text{(Eq 6)}$$

The inversion of boundary conditions gives:

$$T(x,0) = 0 \text{ and } \frac{\partial T(x,p)}{\partial x}\Big|_{x=0} = \frac{\rho VL}{kp} \quad \text{(Eq 7)}$$

and

$$g(x,p) = 0 \quad \text{(Eq 8)}$$

where p is the Laplace transform variable.

The solution to Eq 6 gives the result:

$$T(x,p) = A\exp\left(-\frac{x}{\sqrt{\alpha}}([b-\sqrt{b^2+p})\right) + B\exp\left(-\frac{x}{\sqrt{\alpha}}(b+\sqrt{b^2+p})\right) - \frac{I_0\delta\alpha}{kp}\left[\frac{\exp(-\delta x)}{c^2-(b^2+p)}\right] \quad \text{(Eq 9)}$$

where $b = V/2\sqrt{\alpha}$, $c = b - \delta\sqrt{\alpha}$, and A and B are constants of integration. Using the boundary condition in Eq 3, it yields:

$$A = 0$$

Furthermore, substitution of boundary condition in Eq 3 gives:

$$B = \frac{\sqrt{\alpha}}{b+\sqrt{b^2+p}}\left[\frac{I_0\delta^2\alpha}{kp(c^2-b^2-p)} - \frac{\rho VL}{kp}\right]$$

Therefore, the complete solution to the transformed equation is:

$$T(x,p) = \frac{\sqrt{\alpha}}{b+\sqrt{b^2+p}}\left[\frac{I_0\delta^2\alpha}{kp(c^2-b^2-p)} - \frac{\rho VL}{kp}\right] \exp\left[-\frac{x}{\sqrt{\alpha}}(b+\sqrt{(b^2+p)})\right] - \frac{I_0\delta\alpha}{kp}\left[\frac{\exp(-\delta x)}{c^2-b^2-p}\right] \quad \text{(Eq 10)}$$

In inversion of the transformed solution, the difficulty arises because of the first term, which is a rather complicated function of the subsidiary variable p. The more elegant method is to make use of the observation that the first term can be written as the indefinite integral, that is:

$$f(x,p) = -\int_0^x \left[\frac{I_0\delta^2\alpha}{kp(c^2-b^2-p)} - \frac{\rho VL}{kp}\right] \exp\left(-\frac{x}{\sqrt{\alpha}}(b+\sqrt{b^2+p})\right)dx$$

$$f(x,p) = -\int_0^x g(x,p)dx$$

The inverse transformation of this function may be carried out in the following manner:

$$L^{-1}f(x,p) = -L^{-1}\int_0^x g(x,p)dx = -\int_0^x L^{-1}g(x,p)dx$$

where L^{-1} is the inverse Laplace transformation. The function $g(x,p)$ is easier to invert than the function $f(x,p)$, but involves indefinite integration after the inversion process. The result of this procedure for inverting the solution is the same as that obtained in the following method of expansion into partial fractions.

Using the relationship:

$$L^{-1}[\varphi(P+a)] = e^{-at}L^{-1}[\varphi(p)]$$

It yields:

$$L^{-1}\left[\frac{\sqrt{\alpha}}{b+\sqrt{b^2+p}}\frac{I_0\delta^2\alpha}{kp(c^2-b^2-p)}\exp\left(-\frac{x}{\sqrt{\alpha}}\left(b+\sqrt{b^2+p}\right)\right)\right] =$$
$$-\exp\left[-\left(\frac{bx}{\sqrt{\alpha}}+b^2t\right)\right]L^{-1}\left[\frac{I_0\delta^2\alpha\exp(-qx)}{k(p-b^2)(p-c^2)(q+b\sqrt{\alpha})}\right]$$

where $q^2 = b/\alpha$, $b = V/2\alpha$, and $c = b - \delta\sqrt{\alpha}$.

This expression can be expanded into partial fractions using the residual theorem:

$$-\frac{I_0\delta^2}{k\alpha}\exp\left[-\left(\frac{bx}{\sqrt{\alpha}}+b^2t\right)\right]L^{-1}\left[\frac{\alpha\sqrt{\alpha}\exp(-cx)}{2b(b^2-c^2)(q+b\sqrt{\alpha})^2}\right.$$
$$-\frac{\alpha^2(5b^2-c^2)\exp(-qx)}{4b^2(b^2-c^2)^2(q+b\sqrt{\alpha})}+\frac{\alpha^2\exp(-qx)}{4b^2(b^2-c^2)(q-b\sqrt{\alpha})}$$
$$\left.-\frac{\alpha^2\exp(-qx)}{2c(b+c)(b^2-c^2)(q-c\sqrt{\alpha})}+\frac{\alpha^2\exp(-qx)}{2c(b-c)(b^2-c^2)(q+c\sqrt{\alpha})}\right]$$

which gives on inversion and after many algebraic manipulations:

$$\frac{I_0\delta\sqrt{\alpha}}{2\rho C_p(\alpha\delta-V)}\left\{4\sqrt{t}\,\text{ierfc}\left(\frac{x}{2\sqrt{\alpha t}}+b\sqrt{t}\right)+\frac{3b^2+c^2}{2b(b^2-c^2)}\right.$$
$$\text{erfc}\left(\frac{x}{2\sqrt{\alpha}t}+b\sqrt{t}\right)+\frac{1}{2b}\exp\left(-\frac{2bx}{\sqrt{\alpha}}\right)\text{erfc}\left(\frac{x}{2\sqrt{\alpha}t}-b\sqrt{t}\right)$$
$$-\frac{1}{(b-c)}\exp\left[-[\delta x+(b^2-c^2)t]\right]\text{erfc}\left[\left(\frac{x}{2\sqrt{\alpha t}}+c\sqrt{t}\right)\right]$$
$$\left.-\frac{1}{(b+c)}\exp\left[\frac{x}{\sqrt{\alpha}}(b+c)+(b^2-c^2)t\right]\text{erfc}\left(\frac{x}{2\sqrt{\alpha t}}-c\sqrt{t}\right)\right\} \quad \text{(Eq 11)}$$

The second part of the term in the transformed solution can be inverted in a similar manner:

$$L^{-1}\left[\frac{\rho VL\sqrt{\alpha}}{kp}\frac{\exp\left(-\frac{x}{\sqrt{\alpha}}(b+\sqrt{b^2+p})\right.}{(b+\sqrt{b^2+p}}\right] =$$
$$\frac{\rho VL}{4kb^2}\exp\left[-\left(b^2t+\frac{bx}{\sqrt{\alpha}}\right)\right]$$
$$L^{-1}\left[\frac{\exp(-qx)}{(q-b\sqrt{\alpha})}-\frac{\exp(-qx)}{q+b\sqrt{\alpha})}-\frac{2b}{\sqrt{\alpha}}\frac{\exp(-qx)}{(q+b\sqrt{\alpha})^2}\right]$$

which after transformation gives:

$$\frac{\rho VL}{4bk}\left\{4b\sqrt{\alpha t}\,\text{ierfc}\left(\frac{x}{2\sqrt{\alpha t}}+b\sqrt{t}\right)-\sqrt{\alpha}\,\text{erfc}\left(\frac{x}{2\sqrt{\alpha t}}+b\sqrt{t}\right)\right.$$
$$\left.+\sqrt{\alpha}\exp\left(\frac{-2bx}{\sqrt{\alpha}}\right)\text{erfc}\left(\frac{x}{2\sqrt{\alpha t}}-b\sqrt{t}\right)\right\} \quad \text{(Eq 12)}$$

Finally, the term:

$$L^{-1}\left[\frac{I_0\alpha\delta}{k}\frac{\exp(-\delta x)}{p(p+b^2-c^2)}\right] =$$
$$\frac{I_0\delta}{\rho C_p}\exp(-\delta x)\,L^{-1}\left[\frac{1}{(c^2-b^2)(p+b^2-c^2)}-\frac{1}{(c^2-b^2)p}\right]$$

or

$$L^{-1} = \frac{I_0\delta\sqrt{\alpha}}{\rho C_p(\alpha\delta-V)}\left[\frac{\exp\left[-(\delta x+(b^2-c^2)t)\right]}{(b-c)}-\frac{\exp(-\delta x)}{(b-c)}\right] \quad \text{(Eq 13)}$$

where $b - c = \delta\sqrt{\alpha}$.

Substitution of all these terms (Eq 11, 12, and 13) into Eq 10 gives the complete solution of Eq 1 yields:

$$T(x,t) = \frac{I_0\delta\sqrt{\alpha}}{2\rho C_p(\alpha\delta-V)}\left\{4\sqrt{t}\,\text{ierfc}\left(\frac{x}{2\sqrt{\alpha t}}+b\sqrt{t}\right)\right.$$
$$+\frac{3b^2+c^2}{2b(b^2-c^2)}\text{erfc}\left(\frac{x}{2\sqrt{\alpha t}}+b\sqrt{t}\right)+\frac{1}{2b}\exp\left(-\frac{2bx}{\sqrt{\alpha}}\right)$$
$$\text{erfc}\left(\frac{x}{2\sqrt{\alpha t}}-b\sqrt{t}\right)+\frac{1}{(b-c)}\exp\left[-(\delta x+(b^2-c^2)t)\right]$$
$$\text{erfc}\left[-\left(\frac{x}{2\sqrt{\alpha t}}+c\sqrt{t}\right)\right]+\frac{1}{(b+c)}\exp\left[-\frac{x}{\sqrt{\alpha}}(b+c)+(b^2-c^2)t\right]$$
$$\left.\text{erfc}\left(\frac{x}{2\sqrt{\alpha t}}-c\sqrt{t}\right)-\frac{2}{(b-c)}\exp(-\delta x)\right\}$$
$$-\frac{\rho VL}{4bk}\left\{4b\sqrt{\alpha t}\,\text{ierfc}\left(\frac{x}{2\sqrt{\alpha t}}+b\sqrt{t}\right)-\sqrt{\alpha}\right.$$
$$\left.\text{erfc}\left(\frac{x}{2\sqrt{\alpha t}}+b\sqrt{t}\right)+\sqrt{\alpha}\exp\left(-\frac{2bx}{\sqrt{\alpha}}\right)\text{erfc}\left(\frac{x}{2\sqrt{\alpha t}}-b\sqrt{t}\right)\right\}$$